Computational model of a circulation current that controls electrochemical properties in the mammalian cochlea

Fumiaki Nin[a,b], Hiroshi Hibino[c,1], Shingo Murakami[a,d], Toshihiro Suzuki[b], Yasuo Hisa[b], and Yoshihisa Kurachi[a,d,1]

[a]Division of Molecular and Cellular Pharmacology, Department of Pharmacology and [d]Center for Advanced Medical Engineering and Informatics, Osaka University, Osaka 565-0871, Japan; [b]Department of Otolaryngology-Head and Neck Surgery, Kyoto Prefectural University of Medicine, Kyoto 602-8566, Japan; and [c]Department of Molecular Physiology, Niigata University Medical School, Niigata 951-8510, Japan

Edited* by A. J. Hudspeth, The Howard Hughes Medical Institute, New York, NY, and approved April 18, 2012 (received for review December 5, 2011)

Sound-evoked mechanical stimuli permit endolymphatic K^+ to enter sensory hair cells. This transduction is sensitized by an endocochlear potential (EP) of +80 mV in endolymph. After depolarizing the cells, K^+ leaves hair cells in perilymph, and it is then circulated back to endolymph across the lateral cochlear wall. In theory, this process entails a continuous and unidirectional current carried by apical K^+ channels and basolateral K^+ uptake transporters in both the marginal cell and syncytial layers of the lateral wall. The transporters regulate intracellular and extracellular [K^+], allowing the channels to form K^+ diffusion potentials across each of the two layers. These diffusion potentials govern the EP. What remains uncertain is whether these transport mechanisms accumulating across diverse cell layers make up a continuous circulation current in the lateral wall and how this current might affect the characteristics of the endolymph. To address this question, we developed an electrophysiological model that incorporates channels and transporters of the lateral wall and channels of hair cells that derive a circulation current. The simulation replicated normal experimental EP values and reproduced experimentally measured changes in the EP and intra- and extracellular [K^+] in the lateral wall when different transporters and channels were blocked. The model predicts that, under these different conditions, the circulation current's contribution to the EP arises from different sources. Finally, our model also accurately simulated EP loss in a mouse model of a chloride channelopathy associated with deafness.

hearing | homeostasis | inner ear | ion transport | modeling

The mammalian cochlea is filled with two distinct extracellular solutions, perilymph and endolymph. Whereas perilymph is similar to other extracellular fluids of the body, endolymph exhibits a high [K^+] of 150 mM and an endocochlear potential (EP) of +80 mV relative to either blood plasma or perilymph (1). The cell bodies of sensory hair cells lying on the basilar membrane are bathed in perilymph, whereas hair bundles are exposed to endolymph. Deflection of the stereocilia by acoustic stimuli results in opening of mechanoelectrical transduction (MET) channels at their tips. This process permits K^+ to enter the hair cells, thereby depolarizing them (2). The EP sensitizes hair cells by enhancing driving force for K^+ entry (3). K^+ then passes through the basolateral membranes of hair cells and into the perilymph, where it is thought to be circulated back to the endolymph by K^+ transport mechanisms in the lateral wall (Fig. 1*A*) (4–7). Disruption of K^+ transport mechanisms causes deafness in mice and humans (6, 8).

This net flux of K^+, which has variously been described as the circulation current or the K^+ cycling or K^+ recycling pathway (4–11), might occur even in the resting state (3). In which case, such an idling current could both maintain electrochemical homeostasis within the cochlea and permit hair cells to respond rapidly to mechanical stimuli (3, 7, 12, 13). An analogous dark current exists in retinal photoreceptors (14).

The lateral cochlear wall is considered to functionally consist of two layers (Fig. 1*B*) (4, 5, 7, 15). One layer is a monolayer of marginal cells within the stria vascularis; the apical surfaces of these cells face the endolymph. The other layer is a syncytium that comprises intermediate and basal cells in the stria and fibrocytes in the spiral ligament. The three cell types are interconnected through gap junctions, and thus, they bear similar electrochemical properties (11). The syncytial layer exposes its basolateral surface, which contains fibrocytes, to the perilymph. The two layers sandwich numerous capillaries and an extracellular space called the intrastrial space (IS) that has fluid that shows a low [K^+] and a potential similar to the EP (16, 17) (Fig. 1*B*). This positive IS potential (ISP) is a major contributor to the EP in normal conditions (16, 18).

We have recently shown that the EP largely stems from two K^+ diffusion potentials (i.e., K^+ equilibrium potential E_K) in the lateral wall (18, 19) (Fig. 1*C*, a). The first K^+ diffusion potential dominates the ISP and is established by Ba^{2+}-sensitive K^+ channels, Kir4.1, located at the apical membranes of intermediate cells of the syncytial layer (15, 16, 20, 21). The low [K^+] in the IS ($[K^+]_{IS}$) is necessary for the large K^+ diffusion potential, and it is maintained by Na^+, K^+-ATPases and Na^+, K^+, 2 Cl^- cotransporter type 1 (NKCC1) expressed on the basolateral membranes of the syncytial and marginal cell layers (22, 23). KCNQ1/KCNE1 K^+ channels on the apical surfaces of marginal cells establish the second diffusion potential, and the amplitude depends on intracellular [K^+] of marginal cells ($[K^+]_{MC}$) (24, 25).

The work by Zidanic and Brownwell (12) measured a graded potential by serially advancing an electrode that was inserted into the perilymph. This measurement is experimental evidence for the existence of a continuous circulation current within the cochlea (13). Because the graded potential was modulated by acoustic stimuli (12), MET channels serve as the pathway for the circulation current across the hair cell layer. In the lateral wall, the pathway for the circulation current has been proposed to consist of the apical K^+ channels and basolateral K^+ uptake transporters in the syncytial and marginal cell layers that are crucial for the EP (4–7, 26, 27). Whether and how these separate elements in the lateral wall might assemble to drive the circulation current, however, has not yet been established. Also, the mechanisms and degree by which the circulation current contributes to the maintenance of the EP are not known. The problem is that the critical in vivo experiments that might help to elucidate the relevance of the circulation current to transporter activity regulating the EP are beyond current experimental methods.

In this study, we describe a computational approach. We assumed that the channels and transporters on each of the membranes of the lateral wall interacted and were serially connected with MET channels to form a closed-loop circuit. Our Nin–Hibino–Kurachi (NHK) model not only reproduces the electrophysiologically recorded properties within each compartment of the cochlea but also shows how the circulation current can

Author contributions: F.N., H.H., and Y.K. designed research; F.N., H.H., and S.M. performed research; T.S. and Y.H. contributed new reagents/analytic tools; F.N., H.H., S.M., and Y.K. analyzed data; and F.N., H.H., S.M., and Y.K. wrote the paper.

The authors declare no conflict of interest.

*This Direct Submission article had a prearranged editor.

[1]To whom correspondence may be addressed. E-mail: hibinoh@med.niigata-u.ac.jp or ykurachi@pharma2.med.osaka-u.ac.jp.

This article contains supporting information online at www.pnas.org/lookup/suppl/doi:10.1073/pnas.1120067109/-/DCSupplemental.

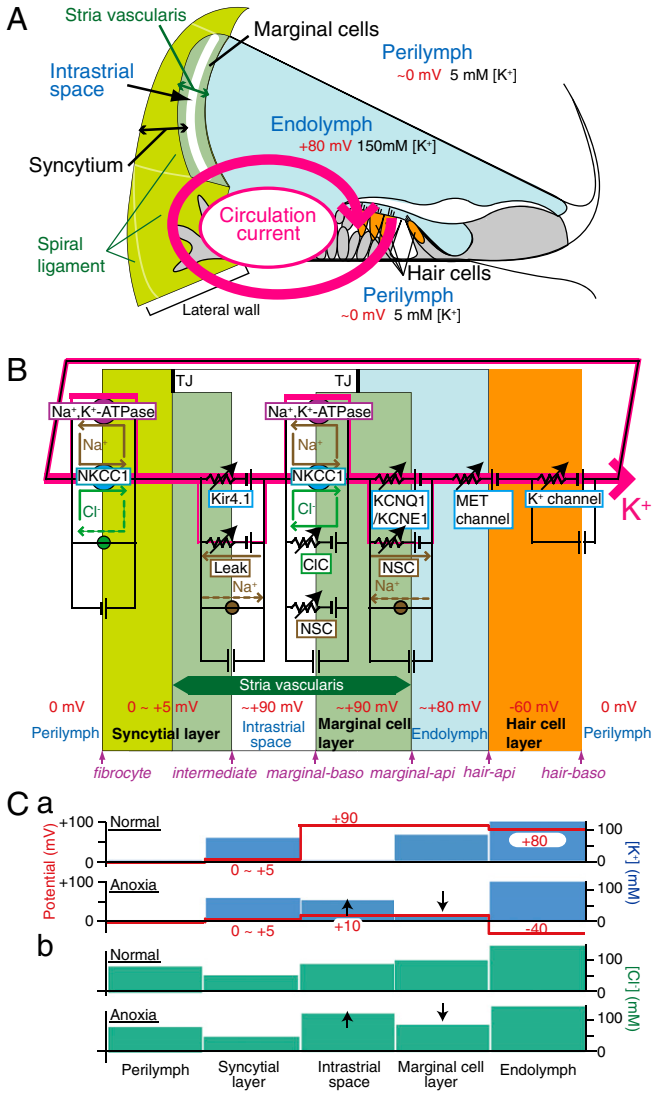

Fig. 1. Key elements of the NHK model. (*A*) Structure of the cochlea and the concept underlying the circulation current. The circulation current (pink arrow) unidirectionally flows through a pathway comprising the endolymph, hair cells, perilymph, and lateral cochlear wall, and it flows back to the endolymph. In normal conditions, this flow would be carried by K^+. (*B*) The electrical circuit and its components used in the modeling. The channels and transporters that are involved in driving the circulation current as well as the potential in each compartment are described. The fibrocytes belong to the spiral ligament (*A*). The stria vascularis contains three cell types: basal cells, intermediate cells, and marginal cells. Basal cells, which are omitted in this scheme, are apposed to the fibrocytes and intermediate cells. Note that the apical and basolateral surfaces of the syncytial layer correspond to the membranes of intermediate cells and fibrocytes, respectively. api, apical; baso, basolateral; ClC, ClC-type Cl^- channels; Leak, leak channels; MET, mechanoelectrical transduction; NKCC1, Na^+, K^+, 2 Cl^- cotransporter type 1; NSC, nonselective cation channels; TJ, tight junction. The circles filled with green and brown indicate the Cl^- and Na^+ transporters, respectively. (*C*) Summary profile of $[K^+]$ (a; blue bars), $[Cl^-]$ (b; green bars), and potential (a; red lines and numbers) of the lateral wall on the basis of the experiments in the work by Nin et al. (18) and Figs. S2*A* and S6*C*. The EP primarily represents the sum of two K^+ diffusion potentials across the apical membranes of the syncytial and marginal cell layers (*C*, a *Upper*) (18). *C*, a *Lower* shows that anoxia causes $[K^+]$ in the IS to increase and $[K^+]$ in marginal cells to decrease, modulating the two K^+ diffusion potentials. Consequently, the EP falls to a negative value. Anoxia also changes $[Cl^-]$ properties (*C*, b). In any condition, the potential of the syncytial layer is constant. In *C*, a and b, up and down arrows during anoxia (*Lower*) indicate increase and decrease of $[K^+]$ or $[Cl^-]$, respectively, compared with normal conditions (*Upper*).

consist of different elements and be involved in the formation of the EP under different conditions.

General Description of the Model

In our model, the circulation current and concentrations of ions in lateral wall compartments were inferred from the function of ion channels and transporters as well as morphological features of the cochlea, which included three layers and three extracellular spaces (28) (Fig. 1*B*). These parameters were obtained from the references tabulated in Table S1. Factors governing the activity of channels and transporters are described in *SI Text*. The model simulated the electrophysiological activity in a 10-μm-thick slice of the cochlea, which corresponded to the width of one row of hair cells and lateral wall cells. All simulations were carried out using the MATLAB program (Mathworks) (*SI Text*).

ISP and EP. According to previous studies (16, 18), ISP and EP are defined by the relations (Eq. **1**)

$$ISP = v_{FC} - v_{IM} \quad [1]$$

and (Eq. **2**)

$$EP = v_{FC} - v_{IM} + v_{MB} - v_{MA}, \quad [2]$$

where the right-hand side terms consist of the potentials of fibrocytes (v_{FC}), intermediate cells (v_{IM}), basolateral surfaces of marginal cells (v_{MB}), and apical surfaces of marginal cells (v_{MA}). All potentials are relative to the perilymph, which is defined as 0 mV. Note that fibrocytes and intermediate cells provide the basolateral and apical surfaces of the syncytial layer, respectively, and v_{FC} was fixed at +3 mV in accordance with experimental data (18).

Circulation Current. We assumed that the circulation current is established by an interplay between channels and transporters on each of the membranes of syncytial, marginal cell and hair cell layers, continuously and unidirectionally flows from endolymph to perilymph, and then returns back to endolymph across all of the six membrane compartments (Fig. 1 *A* and *B*). The membranes are, therefore, part of a closed-loop circuit that provides a pathway for the circulation current. MET channels atop the apical surface of the hair cell layer, which is assumed to have no capacitance (29), were considered the sole route for the circulation current (Fig. 1*B*). Thus, the circulation current, I_{Cir}, always equals the summed MET current, I_{MET} (Eq. **3**):

$$I_{Cir} = -N_{HC} \cdot I_{MET}, \quad [3]$$

where N_{HC} is the number of hair cells. The initial absolute value of the I_{Cir} was set to 3 nA (30).

The work by Davis (3) proposed that the amplitude of the MET current varies in proportion to the potential difference across the apical surfaces of the hair cells, v_{HA}. We assumed that the MET channels permeate only K^+, which dominates the endolymph. These relations are described by (Eq. **4**)

$$v_{HA} = -EP + v_{HB} \quad [4]$$

and (Eq. **5**)

$$I_{MET} = G_{MET} \cdot \left(v_{HA} - \frac{RT}{F} \cdot ln\left(\frac{[K^+]_{EL}}{[K^+]_{HC}} \right) \right), \quad [5]$$

where G_{MET} is the conductance of MET channels, v_{HB} is the potential of the hair cells' basolateral surfaces, $[K^+]_{EL}$ is $[K^+]$ in the endolymph, $[K^+]_{HC}$ is the intracellular $[K^+]$ of the hair cell, R is the gas constant, T is the temperature, and F is the Faraday constant. This conductance was calculated from experimental measurements of the MET current through isolated hair cells and v_{HA} in the resting-state potential (30–33). Eqs. **3–5** indicate that the amplitude of the circulation current depends on the amplitude of the EP.

Membrane Potentials, Currents, and Spatial Ionic Concentrations. I_{Cir} flows into a membrane, and I_M constitutes the sum of currents that pass through channels and transporters on the same membrane. At steady state, I_{Cir} equals I_M for all membranes. However, when either I_{Cir} or I_M varies relative to each other, the membrane potential, v, obeys (Eq. **6**)

$$\frac{dv}{dt} = \frac{1}{C}\frac{dQ}{dt} = \frac{I_{Cir} - I_M}{C}, \quad [6]$$

where Q is the electric charge accumulated on the membrane and C is the capacitance. We used this definition to model the dynamics of membrane potentials (*SI Text* and Fig. S1).

Because the membrane potentials determine the EP (Eq. **2**), they, in turn, modulate I_{Cir} (Eqs. **3–5**). The potentials also directly affect the activity of channels and transporters (*SI Text* and Fig. S1), which further feeds back to I_M (see above). Changes in I_{Cir} and I_M are, therefore, cooperative and rapidly equalize. As a result, the amplitudes of I_{Cir} and I_M are approximately equal on the time scale of our model. In the present study, we, therefore, refer to both currents as circulation current.

In our model, the volumes of all of six extracellular and intracellular spaces of the cochlea are fixed. The $[K^+]$, $[Na^+]$, and $[Cl^-]$ in each space are controlled by ionic currents through the membranes (Eq. **7**):

$$\frac{d[X]}{dt} = \frac{I_{X,In} - I_{X,Out}}{V \cdot F}, \quad [7]$$

where $[X]$ is the ionic concentration, $I_{X,In}$ is the inward current of X, $I_{X,Out}$ is the outward current, and V is the volume of the intra-/extracellular space (Fig. S1). $I_{X,In}$ and $I_{X,Out}$ are the corresponding ionic currents, which are components of I_M and I_{Cir}. When the EP reaches a steady state, all ionic concentrations become constant (i.e., $d[X]/dt = 0$). In this situation, the current across any intra-/extracellular space is also constant and corresponds to I_{Cir} (*SI Text* and Fig. S1). We assumed that the Na^+ fluxes through leak channels and nonselective cation (NSC) channels at the apical membranes of intermediate and marginal cells and the Cl^- flux through NKCC1 at the fibrocytes' membranes were cancelled by the fluxes of Na^+ and Cl^- transporters, respectively. As a result, the net flow across membrane compartments other than the basolateral surface of the marginal cells was solely carried by K^+ in any condition, representing a significant simplification in our model (Fig. 1*B* and *SI Text*).

In summary, Eqs. **2–7** indicate that the circulation current regulates the EP and vice versa. Furthermore, the ionic concentrations of extra-/intracellular spaces depend on the circulation current and the membrane potentials that define the EP. Accordingly, the present model proposes that the circulation current, membrane potentials, and spatial ionic concentrations are coupled.

$[Cl^-]$ Within the Lateral Wall. Although Cl^- homeostasis in the stria vascularis seems to contribute to the EP (10), the precise $[Cl^-]$ of extra- and intracellular spaces of the lateral wall has not been fully elucidated. We, therefore, examined the $[Cl^-]$ profile by using electrodes sensitive to potential and Cl^- in different conditions (*SI Text* and Fig. S2). The measured data are summarized in Fig. 1*C*, b. Briefly, anoxia increased $[Cl^-]$ in the IS ($[Cl^-]_{IS}$) and decreased $[Cl^-]$ in marginal cells ($[Cl^-]_{MC}$), although there seems to be little gradient between these two values in normal conditions (17). This measurement was used to determine various parameters (*SI Text*).

Results

Simulation of Inhibition of K^+ Transport in the Lateral Wall. In living animals, anoxia is likely to interfere with the function of Na^+, K^+-ATPase in the basolateral membranes of marginal cells (22). It also seems probable that it would inhibit the concomitant transporter, NKCC1, to a similar extent (*SI Text* and Fig. S3). The extent of the block of these two transporters by anoxia has not been measured. Moreover, neither the volume of IS in vivo nor the conductance of basolateral NSC channels in marginal cells is known. We, thus, used estimated values (*SI Text*) to simulate the EP and the $[K^+]$ and $[Cl^-]$ in the IS and marginal cells under normal and anoxic conditions. When the NSC conductance and IS's volume were fixed as shown in Table S1 and the activity of both transporters was reduced to 5% of their normal value, the NHK model reasonably reproduced our experimental data (18) (Table 1, *SI Text*, and Figs. S2 and S4).

Fig. 2 illustrates the simulated electrophysiological dynamics of the endolymph, IS, and marginal cells under various conditions. The EP and ISP in normal conditions were +74.6 and +83.1 mV, respectively. Simulation of anoxia caused the EP and ISP to both decrease exponentially but with differing rates and amplitudes. Whereas the EP gradually declined with a time

Table 1. Comparison of simulated results and experimental measurement

	Simulation	Experiment	References
Guinea pigs			
EP*	+74.6 mV	+78.1 ± 4.1 mV (n = 30)	17
ISP*	+83.1 mV	+80.7 ± 11.2 mV (n = 3)	16, 18
$[K^+]_{IS}$*	6.2 mM	4.2 ± 1.3 mM (n = 3)	18
$[K^+]_{MC}$*	128.1 mM	96.0 ± 12.7 mM (n = 3)	18
$[Cl^-]_{IS}$*	91.9 mM	92.8 ± 10.1 mM (n = 3)	Fig. S2*A*
$[Cl^-]_{MC}$*	109.2 mM	117.6 ± 21.5 mM (n = 7)	17
EP under Ba^{2+} block (2 min)†	+16.2 mV	+13.0 ± 2.6 mV (n = 4)	37, Fig. S6*C*
ISP under Ba^{2+} block (2 min)†	+22.0 mV	+29.6 ± 7.0 mV (n = 3)	Fig. S6*C*
EP under anoxia (6 min)†	−41.2 mV	−34.4 ± 10.2 mV (n = 7)	18
ISP under anoxia (6 min)†	+18.2 mV	+17.1 ± 4.3 mV (n = 3)	18
$[K^+]_{IS}$ under anoxia (6 min)†	78.9 mM	73.5 ± 16.6 mM (n = 3)	18
$[K^+]_{MC}$ under anoxia (6 min)†	19.0 mM	14.2 ± 8.0 mM (n = 3)	18
$[Cl^-]_{IS} - [Cl^-]_{MC}$ under anoxia‡	29.5 mM	33.3 ± 4.8 mM (n = 3)	Fig. S2*A*
Barttin KO mice			
EP*	+6.6 mV¶	+12.0 ± 3.1 mV (n = 14)	10

*The steady-state values in normal conditions are shown (Table S2).
†Values for the simulations were determined at the indicated time point after the onset of anoxic or Ba^{2+} block conditions. This time point corresponded to the end point of a period of anoxic or Ba^{2+} block conditions shown in Fig. 2.
‡The maximum difference.
¶The conductance of ClC channels was set to 0.1 nS (Fig. 4).

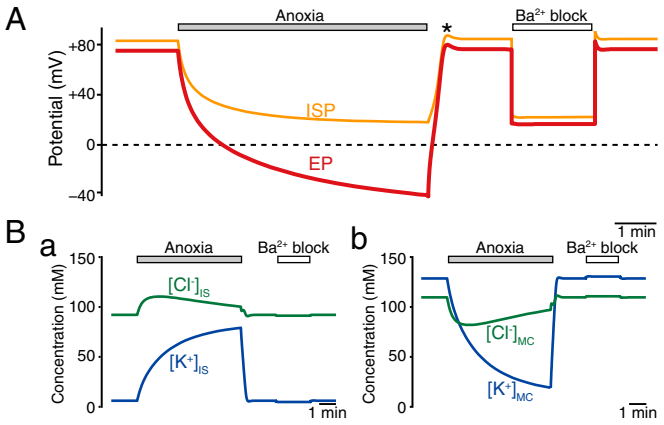

Fig. 2. Simulation of electrochemical properties of the lateral wall and endolymph. Traces exhibit the calculated results of the ISP (orange line in *A*), EP (red line in *A*), $[K^+]$ in IS and marginal cells ($[K^+]_{IS}$ and $[K^+]_{MC}$; blue lines in *B*, a and b), and $[Cl^-]$ in the IS and marginal cells ($[Cl^-]_{IS}$ and $[Cl^-]_{MC}$; green lines in *B*, a and b) in normal, anoxic, and Ba^{2+} block conditions. In this figure and subsequent figures (Fig. 3*A*), the initial values of all of the potentials and concentrations were steady-state values that developed over the course of 3.5 min after the start of the simulation (for the values in the initial 4 min, see Fig. S5 *C* and *D*). The asterisk in *A* marks the overshoots of the potentials after a period of anoxia (18).

constant of $t_{1/2}$ = 75.3 s, the ISP decayed much more rapidly ($t_{1/2}$ = 31.9 s), nearly reaching a plateau within 3 min (Fig. 2*A*). At all times, the EP hyperpolarized more than the ISP. The values of the EP and ISP after 6 min of anoxia were −41.2 and +18.2 mV, respectively. Of note, similar negative EP values were recorded experimentally (34, 35) (Fig. 1*C*, a). On recovery from anoxia, with restoration of both transporters to full activity, both the ISP and EP recovered and briefly exhibited slight overshoots of ∼7.5 mV before returning to their initial values (18) (Fig. 2*A*). During this simulation of anoxia, the ion concentrations in the compartments of the lateral wall also changed dramatically (Fig. 2*B*). $[K^+]_{IS}$ increased from 6.2 to 78.9 mM, and $[K^+]_{MC}$ decreased from 128.1 to 19.0 mM; $[Cl^-]_{IS}$ initially increased from 91.9 to 110.6 mM but then fell by 10.3 mM, whereas $[Cl^-]_{MC}$ initially fell from 109.2 to 81.1 mM before rising by 15.5 mM. All of these behaviors of the ISP, EP, and $[K^+]$ and $[Cl^-]$ in the lateral wall were similar to experimental measurements (18) (Fig. 1*C*, Table 1, and Fig. S2*A*). $[Na^+]$ in the IS and inside marginal cells were also followed in the simulation, and they displayed dynamics that were symmetric to the dynamics of $[K^+]$ (Fig. S5*A*). Experimental data for $[Na^+]$ are not yet available.

Vascular perfusion of a Kir4.1 channel blocker, Ba^{2+}, reduced the ISP and EP in a similar manner, and it affected $[K^+]_{IS}$ and $[K^+]_{MC}$ much less than anoxia (18) (Fig. S6*C*). To simulate the effect of Ba^{2+}, we reduced the conductance of Kir4.1 channels at the apical membranes of intermediate cells by 95.5% (Fig. S6 *A* and *B*). At the onset of this condition, both the ISP and EP immediately dropped to +22.0 and +16.2 mV, respectively (Fig. 2*A*), consistent with experimental data (Table 1 and Fig. S6*C*). $[K^+]_{IS}$ and $[K^+]_{MC}$ were minimally affected (Fig. 2*B*). The simulated results (Fig. 2), thus, reproduce the basic feature of experimentally measured electrophysiological dynamics (18).

The successful simulation of these two experimental conditions supports the overall principles of our model. (*i*) There is an interplay of ion transport apparatus on each of the membranes of the lateral wall and hair cells, and these components are serially connected in a closed-loop circuit to represent the circulation current. (*ii*) The circulation current is coupled to all of the elements responsible for the EP, including the membrane potentials of the lateral wall and its spatial ionic concentrations.

Processes Underlying EP Reduction During Anoxia and Ba^{2+} Block. The mechanisms by which the ISP, EP, and ionic concentrations of the lateral wall respond to anoxia and Ba^{2+} block have not yet been elucidated by experiment. We, therefore, addressed this issue in the model.

We examined the ISP and EP by first isolating their constituents: v_{IM}, v_{MB}, and v_{MA} (Fig. 3*A*). On simulated anoxia, the various potentials changed with differing kinetics. v_{IM} depolarized exponentially from −80.1 to −15.2 mV; the kinetics of this change seemed to bear fast and slow time constants. Whereas v_{MB} hyperpolarized from +3.7 mV to a peak of −8.6 mV in 1 min and then gradually returned to the initial value, v_{MA} monotonically depolarized from +12.2 to +57.3 mV. In contrast, simulation of Ba^{2+} block caused all potentials to change simultaneously and rapidly: v_{IM} depolarized from −81.5 to −19.0 mV, v_{MA} hyperpolarized by 2.0 mV, and v_{MB} depolarized by 0.8 mV.

The ISP mirrors v_{IM} (Eq. **1**). Thus, the ISP's responses to simulations of anoxia and Ba^{2+} block result from those responses incurred by v_{IM}. The difference between the EP and ISP is equal to $v_{MB} - v_{MA}$ (Eqs. **1** and **2**). Throughout the duration of simulated anoxia, this difference was mainly attributable to v_{MA}, because its changes were considerably larger than the changes of v_{MB} (Fig. 3*A*). During simulated Ba^{2+} block, because v_{MA} and v_{MB} changed subtly, ISP and EP declined concomitantly (Fig. 2*A*).

Our simulations reveal possible mechanisms by which membrane potentials respond to anoxia and Ba^{2+} block. In our model, K^+ conductance dominates the apical membranes of marginal cells and intermediate cells, whereas Cl^- conductance governs the basolateral surface of marginal cells (Table S1). Ionic concentrations in endolymph and the syncytial layer were nearly constant

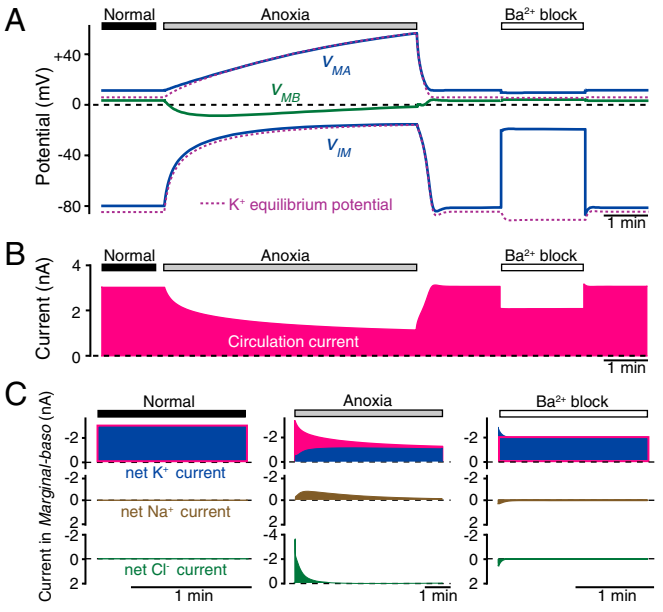

Fig. 3. Simulated membrane potentials and currents in the lateral wall. (*A*) Responses of the membrane potentials in anoxic and Ba^{2+} block conditions (solid lines) (Fig. S5*C*). v_{MA}, v_{MB}, and v_{IM} indicate the potentials across the apical and basolateral membranes of marginal cells and intermediate cells' membranes, respectively. Note that intermediate cells provide the apical surface of the syncytial layer. The purple dotted lines illustrate the change of K^+ equilibrium potentials (E_K) across the apical membranes of marginal cells (*Upper*) and intermediate cells' membranes (*Lower*), which are calculated from $[K^+]$ in endolymph (Table S2) and marginal cells (Fig. 2*B*, b). In the IS (Fig. 2*B*, a) and syncytial layer (Table S2), they are calculated by the relation $E_K = RT/F([K^+]_o/[K^+]_i)$, where $[K^+]_i$ and $[K^+]_o$ are intra- and extracellular $[K^+]$ adjacent to the membrane, respectively. (*B*) The behavior of the circulation current (pink). (*C*) The net K^+, Na^+, and Cl^- currents across the basolateral membranes of marginal cells. Each current is a sum of the respective ionic flux carried by the channels and transporters on the membranes (Fig. S7). The circulation current (pink) underlies the K^+ current (blue) for comparison. The currents shown in this figure are derived from analysis of the data during the periods marked with the top bars in *A* and *B*.

under all conditions (Table S2). Therefore, during anoxia, the drastic reactions of $[K^+]$ and $[Cl^-]$ in the IS and marginal cells (Fig. 2*B*) must play a central role in controlling the membrane potentials. Indeed, the K^+ Nernst potentials (E_K) across the apical membranes of intermediate and marginal cells closely corresponded to the values of v_{IM} and v_{MA} that were simulated using the NHK model (Fig. 3*A*). This result agrees with our previous experimental observation that the ISP as well as the difference between the EP and marginal cells potential could be primarily described as a K^+ diffusion potential, E_K (18, 19) (Fig. 1*C*, a). We found a similar relationship between E_{Cl} and v_{MB} (Fig. S5*B*). During Ba^{2+} block, the dynamics of spatial ionic concentrations are small, barely affecting membrane potentials (Fig. 2*B*). Accordingly, the behavior of v_{IM} clearly departed from the behavior of E_K across the apical membranes of intermediate cells (Fig. 3*A*). Nevertheless, in this condition, v_{IM} rapidly and strongly depolarized, because it is critically determined by the availability of Kir4.1 channels.

It remains unclear how anoxia alters the ionic concentrations of IS and marginal cells and why Ba^{2+} block, in contrast, evokes a relatively minimal effect. One possibility is that the circulation current responds differently during the two conditions. To test this idea, we analyzed the current across the marginal cells' basolateral membranes, which separate these cells from the IS.

Overall, the dynamics of the circulation current always paralleled the dynamics of the EP (Figs. 2*A* and 3*B* and Eqs. **3–5**). Fig. 3*C* elaborates the net K^+, Na^+, and Cl^- currents carried by all channels and transporters at the marginal cells' basolateral membranes (Fig. S7). The circulation current was equal to the sum of all of these currents (*General Description of the Model*). In normal conditions, the membrane current was composed purely of K^+ (Fig. 3*C*). At the onset of anoxia, the membrane passed far more Cl^- than K^+ current. Simultaneously, Na^+ current emerged. Consequently, whereas the Cl^- current was reduced to ~0 nA in 1 min, the Na^+ current increased to a peak of 0.72 nA around 30 s and then gradually decreased. Throughout the duration of anoxia, although the K^+ current continued to gradually rise, its amplitude was always less than the amplitude of the circulation current. These observations indicate that a fraction of the circulation current across the marginal cells' basolateral membranes switched from K^+ to other ions (Fig. S7*D*). Consequently, K^+ influx exceeded K^+ efflux in the IS and vice versa in marginal cells, causing $[K^+]_{IS}$ to increase and $[K^+]_{MC}$ to decrease continuously (Fig. 2*B* and Fig. S1). Similarly, the additional Cl^- and Na^+ currents should evoke a reaction of $[Cl^-]$ and $[Na^+]$ in the two spaces (Figs. 2*B* and Fig. S5). Collectively, the reduction of the EP during anoxia results from a direct modification of the profile of the circulation current.

In contrast, at the onset of Ba^{2+} block, the circulation current immediately decreased by ~1 nA (Fig. 3*B*) because of its dependence on the EP (Eqs. **3–5**). At the marginal cells' basolateral membranes, K^+ flux also reduced as much as the circulation current, but it took ~10 s until this component reached a plateau (Fig. 3*C*). Thus, a small difference in amplitude between the K^+ flux and circulation current occurred transiently, modifying $[K^+]_{IS}$ and $[K^+]_{MC}$ slightly (Fig. 2*B*). The charge imbalance caused by this difference was canceled by the subtle Na^+ and Cl^- fluxes that emerged instantaneously (Fig. 3*C*). Clearly, these additional fluxes underlie the modest alternation of $[Cl^-]$ and $[Na^+]$ in the IS and marginal cells (Fig. 2*B* and Fig. S5).

The simulation of these two conditions shows that the involvement of the circulation current in forming the EP varies in different conditions.

Effects of Dysfunction of Cl^- Flow Across the Lateral Wall. ClC-type Cl^- channels occur in the basolateral membranes of marginal cells. Genetic ablation of their β-subunit barttin impairs the EP and hearing in mice (9, 10). Loss-of-function mutations of the human barttin gene lead to deafness in type IV Bartter syndrome (9, 36). Therefore, Cl^- flow in the lateral wall contributes to the EP. We tested if our model could reproduce reduction of the EP by dysfunction of the Cl^- flow in the marginal cells. We decreased the conductance of ClC channels and then analyzed the steady-state potentials and ionic concentrations in the compartments of the cochlea (Fig. 4).

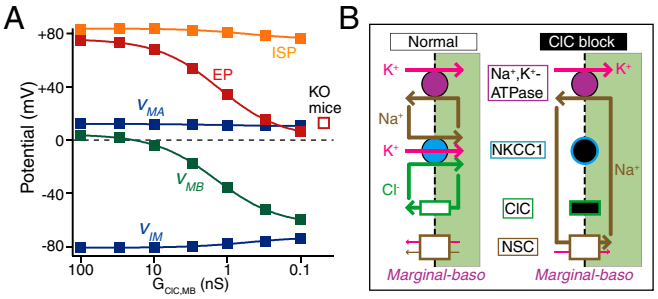

Fig. 4. Effects of dysfunction of Cl^- flow of the lateral wall. Plotted are the steady-state values of the EP, ISP, and membrane potentials (Fig. 3*A* describes abbreviations) as a function of the conductance of ClC-type Cl^- channels (*A*). These potentials represent values that were predicted for a time point 18,000 s into the simulation. This ensured that all potentials represented steady-state values, therefore mimicking unperturbed values that would be measured in living animals that have varying degrees of ClC conductance. The EP measured in barttin KO mice, which lack functional ClC channels (10), is indicated by the open square. *B* illustrates the predicted ionic flows across the basolateral membranes of marginal cells in the normal condition (*Left*) and during block of ClC channels (*Right*). Under normal conditions, NKCC1 cancels the Cl^- flow through ClC channels. During block of ClC channels, Na^+ uptake through the NKCC1 is reduced; consequently, Na^+ inflow is rerouted from NKCC1 to NSC channels, hyperpolarizing v_{MB} (details in *SI Text*). The symbols filled with black indicate the dysfunction of the channels or transporters that is predicted to occur.

As the ClC conductance was reduced, the EP declined (Fig. 4*A*). When the conductance was set to 0.1% of the control (0.1 nS), the EP was +6.6 mV, which is similar to the EP measured in barttin KO mice (+12 mV) (Table 1) (10). Our model, therefore, clearly replicates the relationship between Cl^- homeostasis and the electrochemical properties of the lateral wall and endolymph. Of interest, the ISP remained similar to the ISP of normal conditions. An analysis of the various membrane potentials after ClC conductance reduction revealed little change in v_{MA} but a prominent hyperpolarization of v_{MB} (Fig. 4*A*). The latter element is, therefore, mainly responsible for the pronounced difference between the ISP and EP. Moreover, although simulated ClC channel null conditions had little effect on ionic concentrations in marginal cells (Table S2), at the basolateral surfaces, they evoked an Na^+ influx through NSC channels that markedly increased as the ClC conductance decreased (Fig. 4*B* and Fig. S8). Accordingly, there was hyperpolarization of v_{MB} and also, reduction of the EP stem from this abnormal behavior of the Na^+ current (Fig. 4, *SI Text*, and Fig. S8). Although the circulation current decreased in a manner similar to the EP, it most likely does not directly contribute to the v_{MB} hyperpolarization (Fig. 4*B* and Fig. S8). This mechanism (Fig. 4) may underlie deafness in Bartter syndrome.

Discussion

Not all of the individual elements that make up the structure and function of ion transport systems in the inner ear are known from experimental studies. We have, therefore, taken a theoretical approach to address the question of a circulation current from the endolymph to the perilymph through multiple cell layers and intercellular spaces in the lateral cochlea wall and back to the endolymph again as an element crucial for hearing. Central principles in our model are (*i*) channels and transporters that interact in each of the membranes of the syncytial and marginal cell layers are serially connected to MET channels in hair cells, thereby establishing a unidirectional current pathway, and (*ii*) the circulation current and all of the elements underlying the EP, such as the membrane potentials of the two layers of the lateral wall and their spatial ionic concentrations, are coupled (*General Description of the Model*). A previously described model (27) was able to predict steady-state values of the EP, but it could not

address the dynamics of potentials and ionic concentrations in any compartments of the cochlea. This limitation was primarily because of the absence of spatial ionic concentrations as variables. Our model incorporated these parameters, which were allowed to vary according to ion channels and transporters (Eq. **7** and Fig. S1). In consequence, this model could reproduce both steady-state values and dynamic changes (Fig. 2 and Table 1). The principle elements and concepts underlying the model would, therefore, seem to be valid.

We show that the circulation current affects the electrochemical properties of the lateral wall and EP differently in different conditions (Fig. 3 and Fig. S7). Strikingly, during anoxia, the model predicts that the increase of $[K^+]_{IS}$ and the decrease of $[K^+]_{MC}$—phenomena that largely account for the reduction of the EP (Fig. 1*C*, a) (18)—stem from a direct modification of the circulation current; its predominant charge carrier switches from K^+ to Na^+ and Cl^- at the basolateral membranes of marginal cells (Fig. 3*C* and Fig. S7*D*). In this situation, the additional Na^+ and Cl^- fluxes emerge primarily through NSC and ClC channels (Fig. S7). Thus, these channels are theoretically the constituents of the pathway for the circulation current. This observation had not been suspected from experimental studies, previous models, or conceptual constructs (4–8, 11, 26, 27). However, during Ba^{2+} block, depolarization of v_{IM} directly reduces the EP, thereby decreasing the circulation current (Figs. 2 and 3). In this condition, modulation of the spatial ionic concentrations and membrane potentials by the circulation current seems to be only moderate, and K^+ remains the principle charge carrier (Fig. 3 *A* and *C* and Fig. S7). Finally, our calculations reproduce the EP measured in animal models of a deaf Cl^- channelopathy (Fig. 4 and Fig. S8), indicating not only the robustness of our model but also, its potential use in analysis of other hearing disorders.

An idling current similar to the cochlear circulation current also seems to occur in the vestibular ampulla. The endolymph contains 150 mM $[K^+]$ but a potential of ~0 mV, which is established solely by a cell layer harboring the same ion transport apparatus as the marginal cells (6). Thus, in the cochlea, the marginal cell layer may be sufficient to provide the voltage source for the circulation current. However, to maximize the hair cell sensitivity, the cochlea must additionally acquire the EP, which drives enough current through the circuit. The major source of this system is the apical K^+ diffusion potential in the syncytial layer, which should be much larger than potential of the circulation current located in marginal cells. Consider a situation where the source of the EP was placed parallel to the circuit of the circulation current (i.e., the channels and transporters in the syncytial layer were separated from the lateral wall and directly connected to the hair cells in another circuit). In this case, the voltage supplied by the EP would be reduced rather than effectively added to the hair cells. The double cell layer of the cochlear lateral wall may serve to counter this result and serially integrate the systems of the circulation current and EP in a single circuit.

ACKNOWLEDGMENTS. We thank Drs. I. Findlay and J. A. Fisher for their critical reading of the text. This work is supported by the following research grants and funds: Grant-in-Aid for Scientific Research B 20249012 (to H.H.), the Senri Life Science Foundation (to H.H.), the Ichiro Kanehara Foundation for the Promotion of Medical Sciences and Medical Care (to H.H.), the Mochida Memorial Foundation for Medical and Pharmaceutical Research (to H.H.), the NOVARTIS Foundation (Japan) for the Promotion of Science (to H.H.), the Yujin Memorial Grant (to H.H.), the Takeda Science Foundation (to H.H.), the Naito Foundation (to H.H.), the Global Center of Excellence (COE) Program *in silico* medicine at Osaka University (to F.N., H.H., and Y.K.), a grant for Research and Development of Next-Generation Integrated Life Simulation Software (to Y.K.), Grant-in-Aid for Scientific Research on Innovative Areas 22136002 (to Y.K.), and a grant supporting the Center for Hybrid Medical Engineering (to Y.K.) from the Ministry of Education, Culture, Sport, Science and Technology of Japan.

1. Bekesy G (1952) Resting potentials inside the cochlear partition of guinea pig. *Nature* 169:241–242.
2. Hudspeth AJ (1989) How the ear's works work. *Nature* 341:397–404.
3. Davis H (1961) Some principles of sensory receptor action. *Physiol Rev* 41:391–416.
4. Wangemann P, Schacht J (1996) Homeostasic mechanisms in the cochlea. *Springer Handbook of Auditory Research: The Cochlea*, eds Dallos P, Popper AN, Fay R (Springer, New York).
5. Wangemann P (2006) Supporting sensory transduction: Cochlear fluid homeostasis and the endocochlear potential. *J Physiol* 576:11–21.
6. Hibino H, Kurachi Y (2006) Molecular and physiological bases of the K^+ circulation in the mammalian inner ear. *Physiology (Bethesda)* 21:336–345.
7. Patuzzi R (2011) Ion flow in stria vascularis and the production and regulation of cochlear endolymph and the endolymphatic potential. *Hear Res* 277:4–19.
8. Zdebik AA, Wangemann P, Jentsch TJ (2009) Potassium ion movement in the inner ear: Insights from genetic disease and mouse models. *Physiology (Bethesda)* 24:307–316.
9. Estévez R, et al. (2001) Barttin is a Cl^- channel beta-subunit crucial for renal Cl^- reabsorption and inner ear K^+ secretion. *Nature* 414:558–561.
10. Rickheit G, et al. (2008) Endocochlear potential depends on Cl^- channels: Mechanism underlying deafness in Bartter syndrome IV. *EMBO J* 27:2907–2917.
11. Kikuchi T, Kimura RS, Paul DL, Adams JC (1995) Gap junctions in the rat cochlea: Immunohistochemical and ultrastructural analysis. *Anat Embryol (Berl)* 191:101–118.
12. Zidanic M, Brownell WE (1990) Fine structure of the intracochlear potential field. I. The silent current. *Biophys J* 57:1253–1268.
13. Johnson SL, Beurg M, Marcotti W, Fettiplace R (2011) Prestin-driven cochlear amplification is not limited by the outer hair cell membrane time constant. *Neuron* 70: 1143–1154.
14. Penn RD, Hagins WA (1969) Signal transmission along retinal rods and the origin of the electroretinographic a-wave. *Nature* 223:201–204.
15. Takeuchi S, Ando M, Kakigi A (2000) Mechanism generating endocochlear potential: Role played by intermediate cells in stria vascularis. *Biophys J* 79:2572–2582.
16. Salt AN, Melichar I, Thalmann R (1987) Mechanisms of endocochlear potential generation by stria vascularis. *Laryngoscope* 97:984–991.
17. Ikeda K, Morizono T (1989) Electrochemical profiles for monovalent ions in the stria vascularis: Cellular model of ion transport mechanisms. *Hear Res* 39:279–286.
18. Nin F, et al. (2008) The endocochlear potential depends on two K^+ diffusion potentials and an electrical barrier in the stria vascularis of the inner ear. *Proc Natl Acad Sci USA* 105:1751–1756.
19. Hibino H, Nin F, Tsuzuki C, Kurachi Y (2010) How is the highly positive endocochlear potential formed? The specific architecture of the stria vascularis and the roles of the ion-transport apparatus. *Pflugers Arch* 459:521–533.
20. Takeuchi S, Ando M (1998) Inwardly rectifying K^+ currents in intermediate cells in the cochlea of gerbils: A possible contribution to the endocochlear potential. *Neurosci Lett* 247:175–178.
21. Takeuchi S, Ando M (1999) Voltage-dependent outward K^+ current in intermediate cell of stria vascularis of gerbil cochlea. *Am J Physiol* 277:C91–C99.
22. Nakazawa K, Spicer SS, Schulte BA (1995) Ultrastructural localization of Na,K-ATPase in the gerbil cochlea. *J Histochem Cytochem* 43:981–991.
23. Crouch JJ, Sakaguchi N, Lytle C, Schulte BA (1997) Immunohistochemical localization of the Na-K-Cl co-transporter (NKCC1) in the gerbil inner ear. *J Histochem Cytochem* 45:773–778.
24. Sakagami M, et al. (1991) Cellular localization of rat Isk protein in the stria vascularis by immunohistochemical observation. *Hear Res* 56:168–172.
25. Shen Z, Marcus DC (1998) Divalent cations inhibit IsK/KvLQT1 channels in excised membrane patches of strial marginal cells. *Hear Res* 123:157–167.
26. Quraishi IH, Raphael RM (2007) Computational model of vectorial potassium transport by cochlear marginal cells and vestibular dark cells. *Am J Physiol Cell Physiol* 292: C591–C602.
27. Quraishi IH, Raphael RM (2008) Generation of the endocochlear potential: A biophysical model. *Biophys J* 94:L64–L66.
28. Schuknecht HF (1993) The inner ear. *Pathology of the Ear*, ed Schknecht HF (Lea and Febiger, Philadelphia).
29. Weiss TF, Leong R (1985) A model for signal transmission in an ear having hair cells with free-standing stereocilia. IV. Mechanoelectric transduction stage. *Hear Res* 20: 175–195.
30. Kennedy HJ, Evans MG, Crawford AC, Fettiplace R (2003) Fast adaptation of mechanoelectrical transducer channels in mammalian cochlear hair cells. *Nat Neurosci* 6: 832–836.
31. Dallos P, Santos-Sacchi J, Flock A (1982) Intracellular recordings from cochlear outer hair cells. *Science* 218:582–584.
32. Ashmore JF, Meech RW (1986) Ionic basis of membrane potential in outer hair cells of guinea pig cochlea. *Nature* 322:368–371.
33. van Den Abbeele T, Teulon J, Huy PT (1999) Two types of voltage-dependent potassium channels in outer hair cells from the guinea pig cochlea. *Am J Physiol* 277: C913–C925.
34. Konishi T, Kelsey E, Singleton GT (1967) Negative potential in scala media during early stage of anoxia. *Acta Otolaryngol* 64:107–118.
35. Bosher SK (1979) The nature of the negative endocochlear potentials produced by anoxia and ethacrynic acid in the rat and guinea-pig. *J Physiol* 293:329–345.
36. Birkenhäger R, et al. (2001) Mutation of BSND causes Bartter syndrome with sensorineural deafness and kidney failure. *Nat Genet* 29:310–314.
37. Hibino H, et al. (1997) An ATP-dependent inwardly rectifying potassium channel, K_{AB}-2 (Kir4.1), in cochlear stria vascularis of inner ear: Its specific subcellular localization and correlation with the formation of endocochlear potential. *J Neurosci* 17: 4711–4721.